Chemistry of 1,1,1,5,5,5-Hexafluoro-2,4-pentanedione on Si(100)-2×1

Lucila P. Méndez De Leo, Laurent Pirolli, and Andrew V. Teplyakov*

Department of Chemistry and Biochemistry, University of Delaware, Newark, Delaware 19716

Received: March 12, 2006; In Final Form: May 9, 2006

The surface chemistry of 1,1,1,5,5,5-hexafluoro-2,4-pentanedione (hfacH), a hydrogenated form of the most common ligand in metal and metal oxide deposition, on Si(100)-2×1 has been investigated using multiple internal reflection Fourier transform infrared spectroscopy (MIR-FTIR), Auger electron spectroscopy (AES), thermal desorption mass spectrometry, and computational analysis. The main goal of these studies was to understand if hfacH is a source of fluorine, carbon, and oxygen contamination for a variety of deposition processes where the hfac ligand is involved. In its molecular form, hfacH may potentially have up to 10 isomers including two ketonic and eight enolic forms. One of the enolic forms is shown to be the most stable upon adsorption on a clean Si(100)-2×1 surface at submonolayer coverages at cryogenic temperatures. Even though only the enolic form is present at cryogenic temperatures, at room temperature any of these isomers can exist and all the possibilities of their interaction with the Si(100)-2×1 surface, including several [2 + 2] and [2 + 4] addition pathways as well as O−H dissociation, should be considered. Despite such an array of possibilities, the room-temperature adsorption is governed by the thermodynamic stability of the final addition products between the hfacH and silicon surface. These adducts are stable at room temperature and decompose upon surface annealing.

1. Introduction

Understanding the surface chemistry of 1,1,1,5,5,5-hexafluoro-2,4-pentanedione ($CF_3COCH_2COCF_3$) on a Si(100)-2×1 surface is of great importance for many practical applications. 1,1,1,5,5,5-Hexafluoro-2,4-pentanedione in its dehydrogenated form is utilized as a ligand in some of the most widely used metal and metal oxide deposition precursor molecules. This ligand is most often referred to as hexafluoroacetylacetonate or hfac. It will be referred to in this paper as hfac and its hydrogenated form, 1,1,1,5,5,5-hexafluoro-2,4-pentanedione, will be referred to as hfacH.

The surface chemistry of hfacH is crucial for a thorough understanding of the copper chemical vapor deposition process (CVD) and of a number of atomic layer deposition (ALD) schemes. Although direct deposition of copper onto a silicon substrate is done very rarely for practical purposes, interaction of hfacH with the Si(100)-2×1 surface should provide an excellent set of spectroscopic benchmarks relevant to copper deposition chemistry. These benchmarks may be further used to understand copper deposition on a variety of substrates at the molecular level.

Two of the most promising classes of copper CVD precursors are copper(II) β-diketonates[1,2] and Lewis-base adducts of copper(I) β-diketonates.[3−6] Some time ago CVD of copper was carried out almost exclusively using copper(II) (β-diketonate)$_2$ species; in particular, Cu(II)(hfac)$_2$ was one of the most widely used precursors. However, these precursors are solids, they require high deposition temperatures, and the presence of hydrogen is required for the deposition of the pure copper metal. In this case, clean copper films can only be obtained in a narrow range of temperatures. They are often contaminated with carbon and fluorine because of thermal decomposition of the ligands during deposition.[1,2,4,7] To overcome these difficulties, liquid compounds of higher volatility, such as Lewis-base adducts of copper(I) β-diketonates, can be used.[3−6] Out of the variety of precursor ligands considered, hfac seemed to be the best choice as a β-diketonate.[4] This ligand is often used in a combination with vinyltrimethylsilane (VTMS) as the Lewis base adduct. The resulting precursor molecule, (hfac)Cu^{I}(VTMS), has been reported to form high-quality Cu films with low levels of impurities on Cu,[7] W,[8−11] TiN,[10,12−14] SiO_2,[9,11,13−17] Al,[13,14] Ag,[18] Si_3N_4,[19] and PtSi[20] surfaces.

Previous studies on a copper surface[7] indicate that when (hfac)Cu^{I}(VTMS) is added to the surface, the VTMS, being weakly bonded to the copper, is molecularly desorbed at moderate temperatures, while the hfac, more strongly bound to the copper atom, may have a stronger interaction with the surface. Similar observations were reported on Pt(111)[21] and silica.[15,16,22] The goal of this work is to characterize and manipulate chemical interactions of hfacH with the Si(100)-2×1 surface and to establish a reliable set of spectroscopic benchmarks for the future studies of the hfac-containing precursor molecules on other substrates.

This paper presents and analyses the physisorption, reaction, and desorption of hfacH on Si(100)-2×1. Infrared, Auger electron spectroscopy (AES), and temperature-programmed reaction/desorption (TPR/D) studies together with computational analysis suggest that at a cryogenic temperature of 100 K hfacH adsorbs on a Si(100)-2×1 surface molecularly in its most stable enolic form. Room temperature adsorption favors the formation of the most thermodynamically stable adducts and partial decomposition. Further chemical transformations of the chemisorbed species upon surface annealing are also described.

2. Methods

2.1. Experimental Methods. Two ultrahigh vacuum (UHV) chambers used in the studies described here are located at the University of Delaware. Both chambers have base pressure around 5×10^{-10} Torr. They are both equipped for Auger electron spectroscopy, low-energy electron diffraction (LEED), and surface cleaning using an ion gun. One chamber is coupled

* Corresponding author. Tel.: (302) 831-1969. Fax: (302) 831-6335. E-mail: andrewt@udel.edu.

10.1021/jp061512o CCC: $33.50
Published on Web 07/06/2006

to an infrared spectrometer (Nicolet, Magna 560) set up in a multiple internal reflection mode utilizing a liquid nitrogen cooled external MCT detector. In the infrared measurements, 2048 scans were collected with the resolution of 4 cm^{-1}. First, the background spectrum was collected and then the appropriate dose of the compound of interest was introduced into the UHV chamber using a leak valve and a brief annealing to the desired temperature was performed if needed. The spectrum was then collected at the same temperature as the background. The unshielded mass spectrometer (SRS 200) is used to determine the cleanliness of the dosing compounds in situ. A 25 × 20 × 1 mm^3 trapezoidal sample of Si(100)-2×1 with 45° beveled edges (Harrick Scientific) was used for the multiple internal reflection infrared spectroscopy studies. This sample, polished on both sides, was mounted on a manipulator capable of cooling the sample to 90 K with liquid nitrogen and heating it to above 1150 K using an e-beam heater (McAllister Technical Services).

The other UHV chamber was largely used for temperature-programmed desorption studies. It is equipped with a shielded differentially pumped mass spectrometer (Hiden Analytical) pumped by a dedicated ion pump. A 10 × 10 mm^2 silicon sample polished on one Si(100) surface was cut from a Si(100) wafer (Semiconductor International). During the temperature-programmed desorption studies, the crystal was positioned at approximately 2 mm from a 2 mm aperture in the shield. Heating rate in the TPR/D studies was 2 K/s.

The silicon crystals were prepared by sputtering with Ar^+ for 40 min at room temperature, followed by annealing for 20 min at approximately 1100 K. This procedure leads to a clean and well-ordered Si(100)-2×1 surface as confirmed by AES and LEED.

Argon (Matheson, 99.999%) for surface cleaning was used without additional purification. 1,1,1,5,5,5-Hexafluoro-2,4-pentanedione (hfacH; Alfa Aesar, 99%+) was prepurified by at least 10 freeze−pump−thaw cycles before introduction into the chamber. The purity of the compound was verified in situ by mass spectrometry and the mass spectra obtained were compared with the available database mass spectrum of hfacH.[23] All exposures are reported in Langmuirs (L), where 1 L = 10^{-6} Torr·s. The pressures have not been corrected for ion gauge sensitivity.

2.2. Computational Methods. Electronic structure calculations were performed using the B3LYP hybrid density functional,[24,25] as implemented in the Gaussian 03 suite of programs.[26] The Si(100)-2×1 surface was modeled by a Si_9H_{12} cluster containing one bare single dimer with silicon atoms representing the subsurface terminated by hydrogen to maintain their hybridization. This cluster, though it does not consider interactions with other dimers, has been successfully used previously to investigate chemical reactions on Si(100)-2×1.[27−38] Selected surface structures were also modeled by a $Si_{15}H_{16}$ cluster. The positions of the silicon atoms representing subsurface were not restricted for the single-dimer model. The positions for the atoms representing the third, fourth, and fifth layers in the two-dimer cluster models were fixed to avoid unrealistic distortions as follows: first a two-dimer cluster model $Si_{15}H_{16}$ was fully optimized at the B3LYP/6-31+G(d) level of theory and then the positions of the atoms representing the third, fourth, and fifth layers in this model were fixed and the appropriate adsorbate models were added to this cluster.

The geometry optimizations were performed using a split valence polarized basis set with diffuse functions: 6-311+G(d,p).[39−47] When a two-dimer cluster was considered, a smaller basis set, 6-31+G(d), was used to avoid long computation times. Selected models were also investigated using single-point computations at a B3LYP/6-311+G(d,p) level of theory. In that latest case, energy comparison was made with a single-point computation for the $Si_{15}H_{16}$ cluster. The most stable isomer of hfacH determined based on the studies presented below was fully optimized at the same level of theory as the corresponding attachment or dissociation model. Zero-point vibrational energy (ZPVE) corrections were accounted for in geometry-unrestricted models.

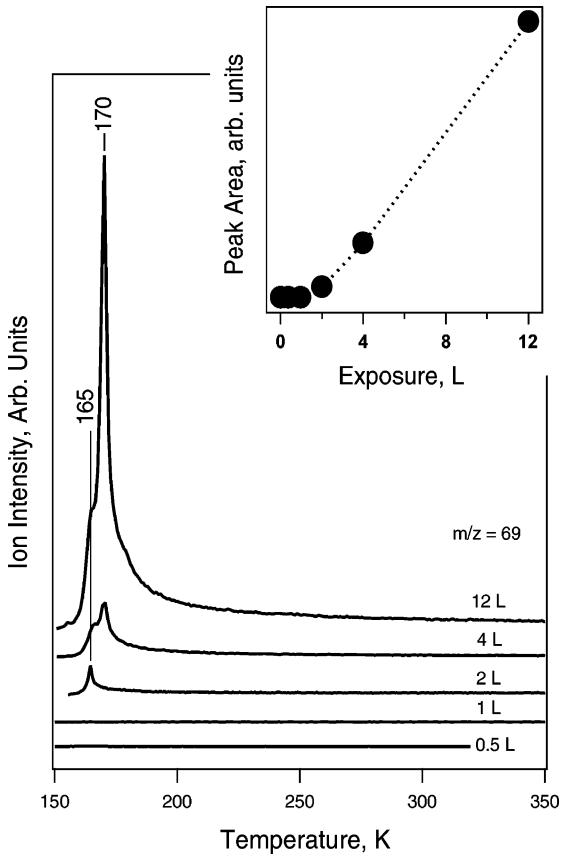

Figure 1. Temperature-programmed reaction/desorption studies of hfacH adsorbed on a Si(100)-2×1 surface at cryogenic temperature (below 130 K). $m/e^+ = 69$ was followed as a function of hfacH exposure. The inset shows the integrated peak areas as a function of the initial exposure.

Vibrational frequency calculations were preformed at the same level of theory as optimization. All calculated minima for fully relaxed models were found to have no imaginary vibrational frequencies. An additional frequency calculation with the clusters terminated with deuterium atoms was performed for each optimized model to identify the absorption peaks arising from hydrogen termination of the model cluster. All calculated vibrational spectra reported were scaled to minimize the known systematic errors. The frequencies were scaled by the factor 0.981, which is the value that gives the best fit of the experimental results performed at cryogenic temperature, when hfacH is physisorbed on the Si(100)-2×1 surface (vide infra).

3. Results and Discussion

First, the bonding and reactivity of hfacH with Si(100)-2×1 have been explored using temperature-programmed desorption (TPD) and MIR-FTIR starting at cryogenic temperatures of 100−130 K, complemented by AES.

A set of TPD spectra for varying exposures of hfacH onto clean and annealed Si(100)-2×1 at cryogenic temperature are

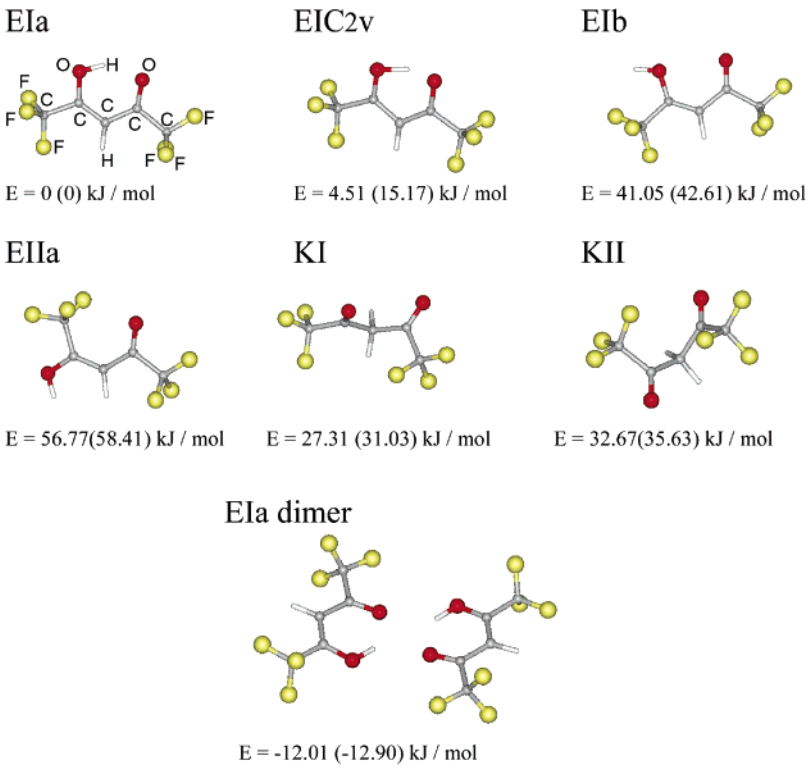

Figure 2. Optimized structures and relative energies (compared to the most stable isomer) for the different possible isomers of hfacH considered in this work. Energies listed under each structure were calculated using the B3LYP/6-311+G(d,p) level of theory. Energies without zero-point vibrational energy (ZPVE) correction are given in parentheses.

shown in Figure 1. $m/z = 69$ was followed in this set of studies because this is the most intense peak in the mass spectrum of the hfacH; however, other mass-to-charge ratios ($m/z = 28$, 44, 119, 139, 208, not shown here) were also followed to confirm that the desorbing molecule is indeed hfacH. The cooling system of the manipulator in the temperature-programmed desorption chamber allows the sample to be cooled to 130 K for adsorption. The molecular desorption was observed for exposures above 1 L, which corresponds to a submonolayer coverage based on coverage profile, a comparison with infrared studies, and with other molecular desorption studies performed using the same experimental setup. The hfacH desorbs at approximately 165 K from the monolayer. Upon further increasing the exposure, this desorption peak seems to split into two features. While the first peak continues to appear around 165 K and saturates quickly, the second peak, recorded at 170 K for a 12 L exposure, grows linearly with the exposure. The activation energy calculated for the peak appearing around 165 K following the first-order kinetics yields a value of 42.1 kJ/mol when the Redhead method with a preexponential factor of 10^{13} s^{-1} is used.[48] This is characteristic of a physisorbed molecule. The inset for Figure 1 shows the integrated desorption peak areas plotted as a function of hfacH exposure. While the majority of the monolayer hfacH adsorbed on a Si(100)-2×1 surface at 100 K desorbes molecularly upon annealing, less than 10% of carbon was observed by AES to remain on the surface after heating it up to room temperature. The observed desorption kinetics is unusual, but it is overall consistent with previous studies of hfacH on reactive surfaces. The multilayer desorbs within the same range of temperatures as was reported for Pt(111)[21] for a higher heating rate. Since the structure of the physisorbed multilayer and its effect on the monolayer was not the target of this investigation, it is sufficient to say that at least part of the hfacH adsorbed in a monolayer desorbes upon annealing. The specific nature of this adsorption is likely very complex; in case of Pt(111), it was suggested to consist of two types of adsorbed hfacH: "lying-flat" and "standing-up".[21] The specific kind of interactions largely depends on the hydrogen-bonding environment and is beyond the scope of the present study. Nevertheless, with the help of the infrared investigation outlined below, it was possible to determine the dominant type of hfacH species adsorbed on Si(100)-2×1 at cryogenic temperatures. To understand the adsorption of hfacH at cryogenic temperatures, computational analysis of the possible isomers of this molecule and corresponding infrared spectra had to be performed. Detailed gas-phase studies are reported in refs 49 and 50. Since we are interested in a condensed phase behavior of hfacH, only selected isomers summarized in Figure 2 were considered here. This set consists of three of the possible eight structures representing the three types of the enolic forms of hfacH, EIa, EIb, and EIIa, with another structure, EIC_{2v}, similar to EIa but having C_{2v} symmetry observed experimentally.[51−53] In fact, the experimental observation was suggested to characterize a superposition of two structures without the C_{2v} symmetry.[50] A similar conclusion was reached on the basis of the NMR studies of isotopically substituted malonaldehyde enol,[54] a compound structurally very similar to hfacH. The set of isomers examined here compares the enolic form of hfacH with an intramolecular hydrogen bond, EIa and EIC_{2v}, the same type of molecule with C−O−H group rotated by 180°, EIb, and one of the models produced by rotation of the C−C bond adjacent to O−H and CF_3 groups by 180°, EIIa. It also contains two possible ketonic isomers, KI and KII, as well as a possible dimer of EIa. As summarized below, the experimental results suggest that the hfacH is adsorbed on Si(100)-2×1 at cryogenic temperatures in its enolic form, and thus, more detailed studies of ketonic isomers were deemed unnecessary. The coverage dependence of the MIR-FTIR spectra of hfacH dosed onto a clean Si(100)-2×1 surface at 100 K is presented in Figure 3. No significant differences in peak positions and relative absorption intensity

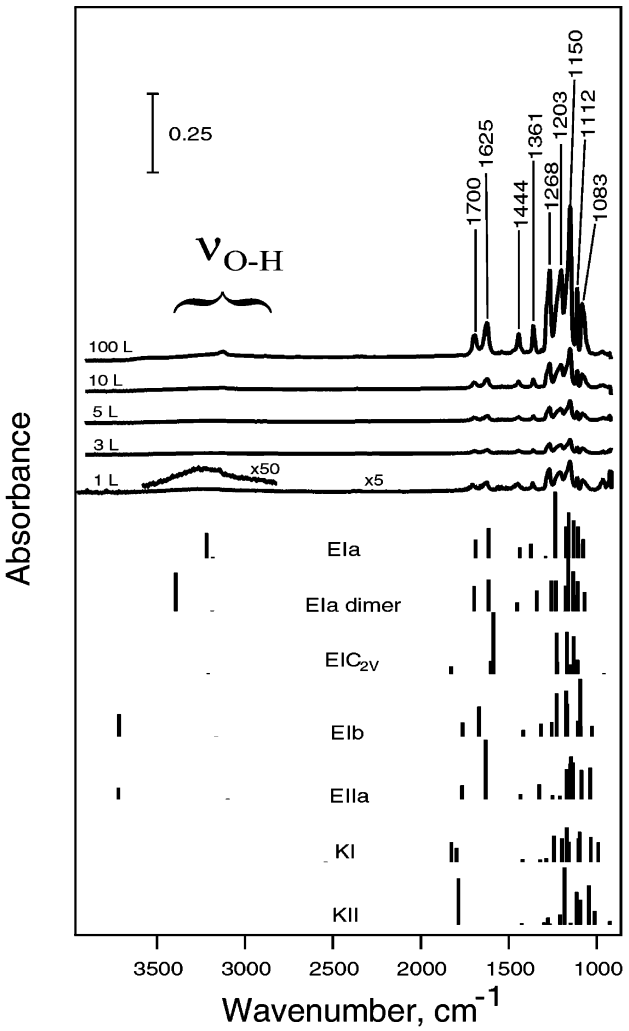

Figure 3. MIR-FTIR spectra of different quantities of hfacH dosed onto the Si(100)-2×1 surface at 100 K and vibrational spectra predicted for different possible isomers of hfacH summarized in Figure 2.

were observed as a function of exposure with the exception of the absorption band corresponding to the O−H stretch above 3000 cm^{-1}. The absolute intensities demonstrated linear increase as a function of exposure. The experimental spectra obtained are very similar to the spectrum of gaseous hfacH obtained by Farkas et al.,[22] as compared in Table 1. Thus, it can be assumed that at this temperature, hfacH is physisorbed on this surface even at submonolayer coverages. The ν_{O-H} is the only adsorption band that exhibits different frequency when exposures of 5 L and below are compared to the large exposures corresponding to multilayer coverage of hfacH. This absorption band is likely very sensitive to the specific chemical surroundings, as hydrogen bonding plays a major role in its appearance.

To determine the nature of the adsorbed isomer of hfacH, Figure 3 also summarizes the predicted infrared spectra for a set of possible isomeric structures shown in Figure 2. Clearly, the enol form of hfacH is dominant at these experimental conditions as the ν_{O-H} is easily observed at all the exposures studied. A careful comparison of the obtained experimental spectra with the predicted vibrational signatures of a variety of possible isomers of hfacH suggests that only the energetically most stable of all the possible enolic forms of hfacH is present on the surface, i.e., structure EIa. The vibrational signatures for structures EIb and EIIa are quite inconsistent with the observed spectrum, especially in the O−H stretch range of 3100−3800 cm^{-1}. This observation confirms that hydrogen bonding plays a significant role in determining the vibrational signatures of the physisorbed hfacH. Interestingly, the infrared spectrum predicted for the hfacH isomer most consistent with the previously published and discussed experimental diffraction data,[51−53] EIC_{2v}, is also qualitatively different from the experimental vibrational spectra observed in these studies. The exact nature of the hydrogen bond can be speculated upon; however, it is clear that non-hydrogen-bonded hfacH molecules would exhibit vibrational spectra different from the ones observed experimentally. To confirm the role of hydrogen bonding, a dimer of EIa hfacH isomer was described computationally. As shown in Figure 2, the gain in stabilization energy is expected to be 12.01 kJ/mol (or 12.90 kJ/mol if the ZPVE is not taken into account) for the dimer or half those values per molecule. However, the ν_{O-H} vibration shown in Figure 3 for a dimer structure is blue-shifted by almost 200 cm^{-1} compared to the intramolecular hydrogen-bonded EIa. In fact, the spectrum predicted for the EIa structure resembles the experimental spectrum of the hfacH condensed on a Si(100)-2×1 surface exceptionally well. This observation by itself does not rule out other possible hydrogen-bonded configurations that could be common in a physisorbed layer of hfacH.

TABLE 1: Peak Positions and Approximate Mode Assignments for hfacH Condensed on a Si(100)-2×1 Surface at Cryogenic Temperature, hfacH in the Gas Phase,[22] and Those Predicted by Computational Investigation

hfacH on Si(100)-2×1[a]	computational investigation[b] model EIa	hfacH(g)[22]	approximate assignments
3125	3219	3136	O−H stretch
	3183	1788	C−H stretch
1700	1689	1692	C═O/C═C stretch
1625	1616	1640	C═C stretch/O−H bend
1444	1438	1445	C═C stretch/C═O stretch/C−H bend
1361	1376	1366	O−H bend/C═C bend/C═O bend
1268	1292	1271	CF_3 stretch/C−H stretch/C═O stretch + C═C stretch
	1236		C−H bend
1203	1175	1227	CF_3 stretch/C−H bend
1150	1161	1188	CF_3 stretch
1112	1131	1092	CF_3 stretch
1083	1106, 1104	912	CF_3 stretch/C−H bend

[a] 100 L at 100 K. [b] Scaled by 0.981.

The correction factor of 0.965 was initially used for comparison of experimental and predicted vibrational spectra. This factor is based on our previous work with the B3LYP method.[55] Once the best fitting spectrum was identified and assigned to be the EIa structure, a slightly better overall fit was obtained with the 0.981 scaling factor. This scaling factor did not alter the similarity of the predicted and experimentally measured spectra significantly and was calculated to match the specific molecule EIa. This factor was calculated as the average of all the scaling factors for all the peaks in the experimental spectrum as compared to the corresponding peaks in the predicted spectrum of the EIa compound in the range of frequencies between 1000 and 2000 cm^{-1}. The O−H stretch vibration was not taken into account in this computation because of the high sensitivity of this absorption band to the specifics of the hydrogen bonding. A 0.981 scaling factor was used for the rest of the studies presented in this paper.

The reactions of hfacH with Si(100)-2×1 at room temperature have been studied using TPR/D, AES, and MIR-FTIR techniques. Figure 4 shows the TPR/D spectra for a saturation exposure of hfacH dosed onto a clean Si(100)-2×1 surface. The only species evolving from the surface correspond to the *m*/*z*

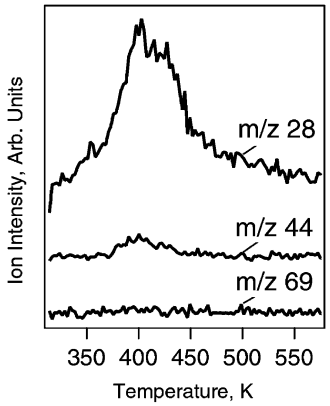

Figure 4. TPR/D investigation of a saturation exposure of hfacH dosed onto Si(100)-2×1 at room temperature.

traces of 28 and 44 (CO and CO_2) observed around 400 K. The rest of the fragments monitored exhibited no desorption features within our signal-to-noise ratio, implying that decomposition dominates surface transformations of hfacH chemisorbed on Si(100)-2×1. It should be noted that the cracking pattern of CO_2 contains the $m/z = 28$ fragment; however, according to the NIST database,[23] the ratio of $m/z = 28$ to $m/z = 44$ intensity for this molecule should be 1:10, while in our studies it is approximately 7:1. In support of the decomposition, AES investigation suggests that even after annealing to 800 K approximately 10% of the original carbon remains on the surface.

MIR FT-IR spectra were obtained for hfacH adsorbed on Si(100)-2×1 at room temperature. Presented in Figure 5a is a spectrum of 1 L of hfacH adsorbed on a clean Si(100)-2×1 surface at 100 K. As this surface is briefly annealed to 200 and 300 K, spectra b and c are produced. Spectra b and c in Figure 5 are essentially identical. The room-temperature adsorption of the saturated monolayer of hfacH yields spectrum 5d. Several major conclusions can be drawn solely on the basis of these experimental investigations. It is apparent that spectra 5b,c contain vibrational signatures of low-intensity absorption features corresponding to ν_{O-H} and ν_{Si-H} as illustrated by the zoom-in in Figure 5b. However, while ν_{O-H} bands are quite pronounced and clearly observed, the ν_{Si-H} is approximately 2 orders of magnitude less intense than other absorption features of this spectrum. Thus, the ν_{Si-H} spectral feature is most likely associated with a very minor product, possibly formed at the defect sites. In other words, O−H dissociation can be ruled out as a major chemisorption pathway for hfacH on Si(100)-2×1. Another undisputable observation is that adsorption of the hfacH at 100 K followed by a brief annealing to room temperature yields a set of surface products that are entirely different from the ones obtained by dosing at room temperature: the combination of $\nu_{C=C}$ and $\nu_{C=O}$ absorption bands clearly observable for the physisorbed hfacH at 1625 and 1700 cm^{-1}, respectively, practically disappears upon annealing, while only a single absorption at 1660 cm^{-1} (corresponding to the $\nu_{C=C}$ vibration) is observed upon hfacH chemisorption at room temperature. It is also important that spectra 5b,c do not exhibit any *strong* $\nu_{C=O}$ absorption bands in the 1500−1700 cm^{-1} region.

Figure 5 also presents a comparison of the experimental spectra with computationally predicted vibrational signatures of different possible structures produced by hfacH as modeled by a single dimer cluster, Si_9H_{12}, and in five cases by a double dimer cluster, $Si_{15}H_{16}$. The list of the structures considered is presented in Figures 6 and 7. All these structures are grouped as I, addition via two C═O bonds; IIA−D, [2 + 4] cycloaddition

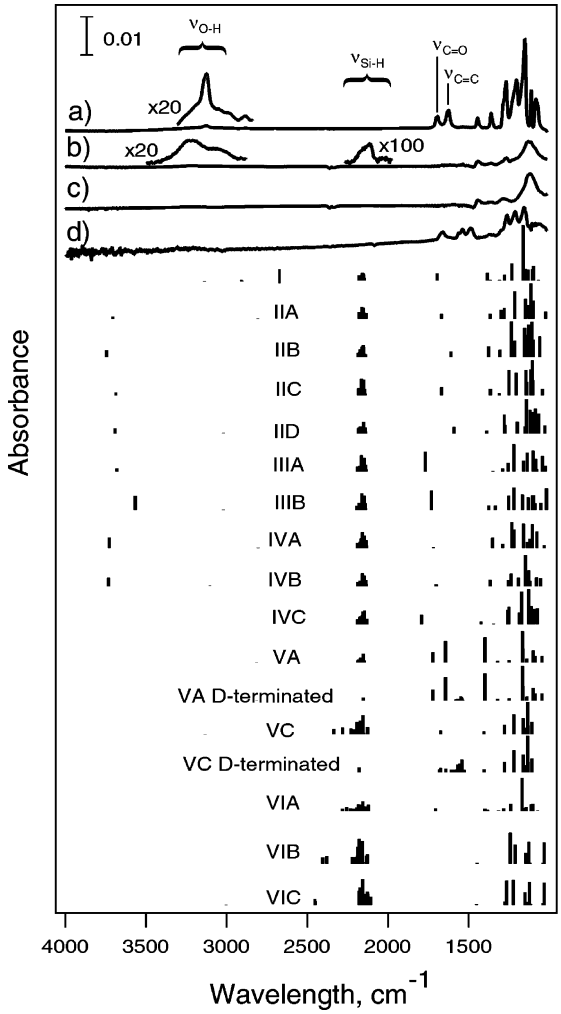

Figure 5. MIR-FTIR spectra of hfacH dosed onto the Si(100)-2×1 surface at the conditions indicated: (a) 1 L dosed at 100 K; (b) 1 L dosed at 100 K and briefly annealed to 200 K; (c) 1 L dosed at 100 K and briefly annealed to 300 K, (d) saturated monolayer (500 L dose) of hfacH at room temperature. Experimental spectra are compared with the predicted infrared spectra for the model structures summarized in Figures 6 and 7. Scaling factor of 0.981 is used for predicted vibrational frequencies.

via one C═O and one C═C double bonds; IIIA,B, [2 + 2] cycloaddition via C═C double bond; and IVA−C, [2 + 2] cycloaddition via C═O double bond. Figure 7 summarizes computational investigation of structures VA−C, the products of O−H dissociation of enolic forms of hfacH, and explores the possibility of hfacH attachment to the two neighboring silicon dimers, VIA−C.

The predicted infrared spectra for all the structures in Figure 5 are based on the optimized configurations for the models in Figures 6 and 7 with silicon clusters terminated by hydrogen atoms. The vibrational features located around 2100 cm^{-1} correspond to this hydrogen termination of silicon cluster. For models VA and VC describing O−H dissociation, Figure 5 also presents the results of vibrational frequency computations with deuterium atoms terminating silicon clusters. In the predicted spectra of the deuterium-terminated models VA and VC, a pronounced ν_{Si-H} absorption band around 2100 cm^{-1} is clearly observed (see Supporting Information for more details). Since none of the experimental spectra presented in Figure 5 exhibits any significant ν_{Si-H} absorption bands (except for minute intensity likely corresponding to surface defect sites), all structures produced by O−H dissociation can be ruled out as

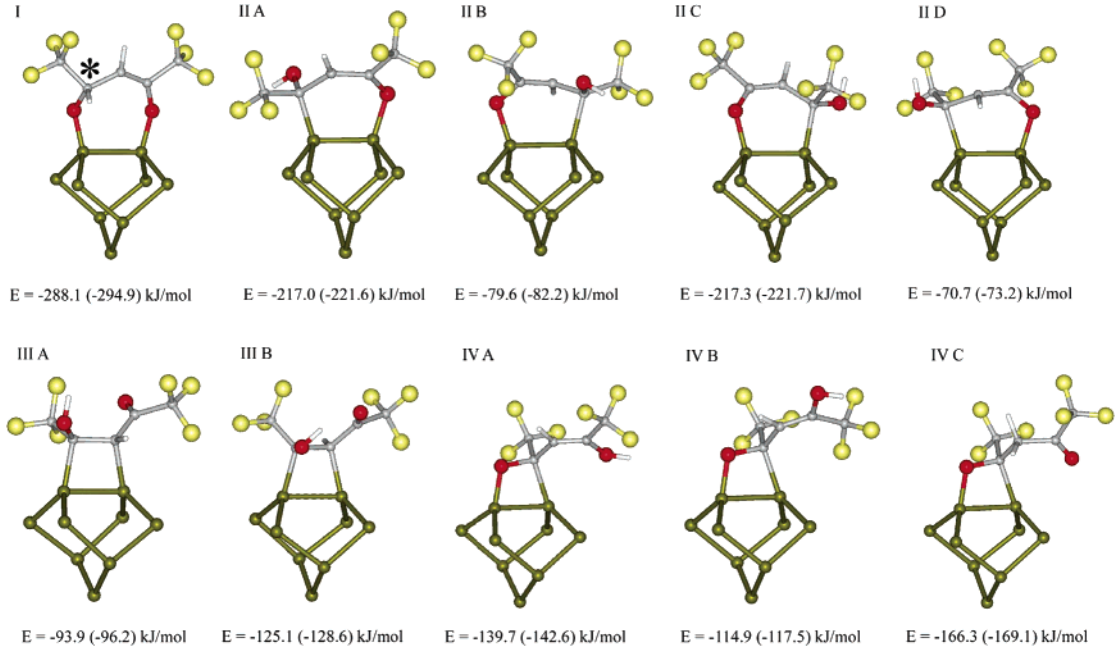

Figure 6. Optimized structures and relative energies (compared to a fully optimized hfacH in the most stable enolic form and a Si_9H_{12} model cluster) for the attachment products of the reaction of hfacH with the Si(100)-2×1 surface considered in this work. Energies listed under each structure were calculated using the B3LYP/6-311+G(d,p) level of theory. Energies without zero-point vibrational energy correction are given in parentheses. Structure I has two isomers because of the optical center denoted with an asterisk (*). The *S*-isomer presented in this figure is 4.1 kJ/mol more stable than the *R*-isomer, and since the infrared spectra of both isomers are very similar, the *R*-isomer was not considered further in this paper. Hydrogen atoms terminating subsurface silicon atoms of the cluster models are omitted for clarity.

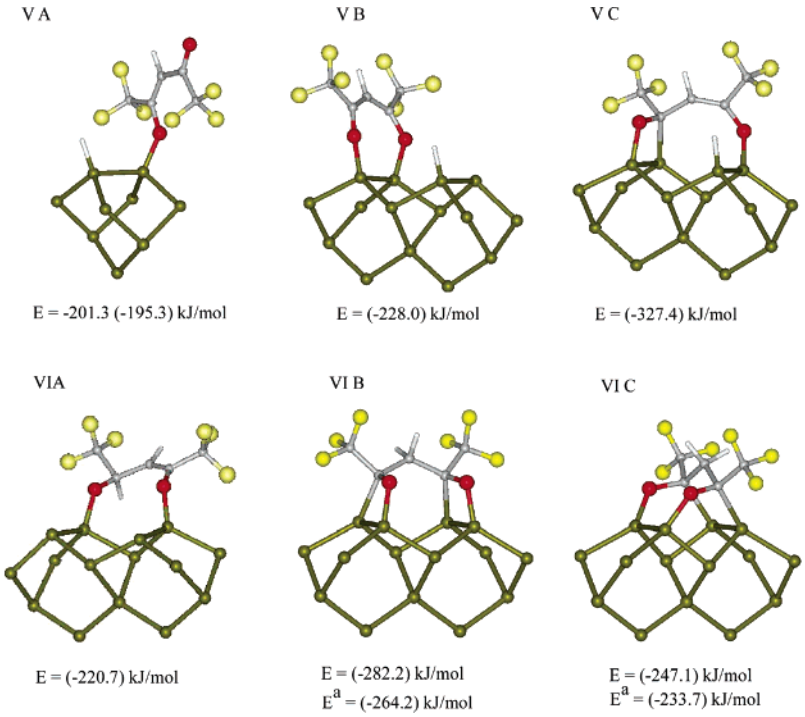

Figure 7. Optimized structures and relative energies (compared to a fully optimized hfacH in the most stable enolic form and a Si_9H_{12} or a $Si_{15}H_{16}$ model cluster) for the dissociation products of the reaction of hfacH with the Si(100)-2×1 surface and for the attachment products over two neighboring dimers considered in this work. Energies listed under each structure were calculated using the B3LYP/6-311+G(d,p) level of theory in the case of one-dimer clusters and the B3LYP/6-31+G(d) level of theory in the case of two-dimer clusters. The hfacH structure was fully optimized at the same level of theory as the corresponding dissociation or attachment configuration. Energies without zero-point vibrational energy correction are given in parentheses. Superscript "a" denotes the single point calculations: B3LYP/6-311+G(d,p)//B3LYP/6-31+G(d). The positions of the cluster atoms representing subsurface silicon were not restricted for single dimer model but were fixed as described in the text for two-dimer models. Hydrogen atoms terminating subsurface silicon atoms of the cluster models are omitted for clarity.

major products of hfacH interaction with the Si(100)-2×1 surface. Structure I seems to be the dominant product of the *room temperature* reaction of hfacH with this silicon surface, since its predicted spectrum aligns quite well with the experimentally observed set of vibrations presented in Figure 5d, except for the doublet around 1500 cm^{-1}. It is also the most stable structure according to the energy optimization studies. However other products may also be present. The existence of

two peaks around 1500 cm^{-1} indicates that further decomposition may take place at room temperature, leading to more complicated products not considered in the present work. Structures IIIA and IIIB are considerably less stable than structure I. The intense $\nu_{C=O}$ absorption feature in the predicted infrared spectra of these models does not match the experimental spectra. Thus, to a great extent, the presence of these structures on the Si(100)-2×1 surface can be disregarded. The presence of structures IIA−D and IVA−C cannot be ruled out completely solely on the basis of the infrared spectra, but all these adducts are at least 70 kJ/mol less stable than structure I, and this number can be even higher than 200 kJ/mol (for example, for structure IID).

The same type of comparison can also be conducted for binding of the hfacH molecule across two silicon dimers of the same dimer row. Despite the fact that infrared spectra predicted for structures I and VIA are very similar, structure I is more stable by ~70 kJ/mol. The infrared spectra of structures VIB and VIC are quite similar to one another, but only structure VIB is comparable to structure I in stability. It should also be noted that both structure VIB and structure VIC are missing the pronounced C−O stretch absorption band observed at room temperature at 1660 cm^{-1} and predicted for structure I. Thus, upon adsorption at room temperature, structure I most likely constitutes the majority of surface species. This observation is also supported by the preliminary study of a similar molecule, 2,2,6,6-tetramethyl-3,5-heptanedione, on Si(100)-2×1 by scanning tunneling microscopy.[56]

It is very interesting to compare the spectrum obtained after dosing at room temperature with the spectra obtained after dosing at cryogenic temperatures followed by brief annealing to room temperature, given in Figure 5. There is a very significant difference between these two types of experiments, indicating that different products are obtained. In the case of hfacH dosed at cryogenic temperatures following the physisorption the hfacH, molecules remaining on a surface react with the silicon surface as the temperature is being increased. It is expected that in this case the kinetically favorable products are obtained as the energy barrier is overcome during the heating procedure, as opposed to the experiments at room temperature, where several products are kinetically accessible, and their mixture, with the energetically most stable one as the major product, is obtained.

The reaction started at cryogenic temperature yields spectra b and c in Figure 5. These spectra are characterized by the absence of $\nu_{C=O}$ and $\nu_{C=C}$ bands of significant intensity and by the presence of ν_{O-H}. According to these observations, the only structures that can potentially be present on a surface following hfacH adsorption at 100 K and brief annealing to 200 or 300 K are IIA−D and IVA,B. The positions of the ν_{O-H} absorption bands in the predicted spectra do not align well with the experimentally observed spectra. However, as was pointed out above, these transitions are the most sensitive to hydrogen bonding, and accurate representation of this type of interaction will only be possible to address by significantly larger and more complex computational models, which is beyond the scope of this paper. Despite the fact that structures IIA and IIC are the most stable among the structures of the type II or IV, the vibrational spectra predicted for all structures of the type II are not consistent with the experimentally recorded spectrum. They all exhibit absorption bands of significant intensity corresponding to carbon−oxygen stretch ν_{C-O} in the 1600−1700 cm^{-1} spectral region. Similar analysis rules out structure IVC. It appears that structures IVA and IVB are the most likely candidates to be responsible for the spectrum collected after adsorbing hfacH at cryogenic temperatures and briefly annealing the surface to 300 K. It is possible that other structures, for example VIB and VIC, are present in this mixture. At least their presence cannot be ruled out based solely on the experimental results presented here.

It is also noteworthy that the most thermodynamically stable structures (I, VIA−C) can only be obtained by chemical transformation of both C═O entities in their ketonic form while both structures IVA and IVB contain an enolic oxygen. Thus, the mechanism of kinetic hfacH addition to the Si(100)-2×1 surface that is initiated at low temperature should start with the enolic form observed to be present at the beginning of this transformation, while the thermodynamically driven room-temperature addition proceeds with the formation of the most stable surface product, even though it does require both C═O groups to be in a ketonic form.

Conclusions

Complex thermal transformations of hfacH on a Si(100)-2×1 surface have been investigated by thermal desorption, infrared spectroscopy, and Auger electron spectroscopy with the purpose of understanding chemisorption configurations for hfacH on this surface as a function of the surface temperature and to determine the pathways of thermal decomposition of the chemisorbed hfacH. Partial explanation of this chemistry was given using a computational analysis of possible configurations of the physisorbed hfacH and of the most probable chemisorption models. hfacH physisorbs molecularly on Si(100)-2×1 when dosed at cryogenic temperatures of 100−130 K, even at submonolayer coverages. The proposed intramolecular hydrogen-bonded model explains all the features of the experimental vibrational spectrum, but other, more complicated hydrogen-bonded structures involving several hfacH molecules may also be responsible for the experimentally obtained spectrum.

The thermal chemistry of hfacH on Si(100)-2×1 depends drastically on the experimental conditions. If hfacH is adsorbed at cryogenic temperatures of 100−130 K and then the temperature of the surface is increased, the major reaction pathway is molecular desorption. The chemistry of the species remaining on the surface seems to be largely governed by kinetics considerations and leads to the formation of species of the type IVA and IVB. On the other hand, if hfacH is dosed at room temperature, the mixture of surface adducts formed is dominated by the most thermodynamically stable structures. These surface adducts decompose upon surface annealing, with partial decomposition observed even at room temperature. Thus, hfacH could potentially be a major source of surface fluorine, carbon, and oxygen for the room-temperature processes, while cryogenic conditions actually allow the majority of hfacH to desorb.

Acknowledgment. Acknowledgment is made to the National Science Foundation (CHE-0313803) for the support of this research. A.V.T. would also like to thank Prof. Brian Willis (Department of Chemical Engineering) and Dr. Olga Dmitrenko (Department of Chemistry and Biochemistry, University of Delaware) for useful discussions.

Supporting Information Available: Graphics of the various structures discussed in the text and their energies predicted using B3LYP/6-311+G(d,p) and B3LYP/6-31+G(d); tables giving the center number, atomic number and type, coordinates, frequency, and IR intensities predicted for these structures. This material is available free of charge via the Internet at http://pubs.acs.org.

References and Notes

(1) Hemmet, R. L. V.; Spendlove, L. B.; Sievers, R. E. *J. Electrochem. Soc.* **1965**, *112*, 1123.
(2) Temple, D.; Reisman, A. *J. Electrochem. Soc.* **1989**, *136*, 3525.
(3) Shin, H. K.; Chi, K. M.; Hampden-Smith, M. J.; Kodas, T. T.; Farr, J. D.; Paffett, M. *Adv. Mater* **1991**, *3* (5), 246−248.
(4) Shin, H. K.; Chi, K. M.; Hampden-Smith, M. J.; Kodas, T. T.; Farr, J. D.; Paffett, M. *Chem. Mater* **1992**, *4*, 788−795.
(5) Norman, J. A. T.; Muratore, B. A.; Dyer, P. N.; Roberts, D. A.; Hochberg, A. K.; Dubois, L. H. *Mater. Sci. Eng. B* **1993**, *17*, 87−92.
(6) Norman, J. A. T.; Muratore, B. A. Volatile liquid precursors for the chemical vapor deposition of copper. US Patent, application 19920204, 1992.
(7) Girolami, G. S.; Jeffries, P. M.; Dubois, L. H. *J. Am. Chem. Soc.* **1993**, *115* (3), 1015−1024.
(8) Jain, A.; Chi, K. M.; Kodas, T. T.; Hampden-Smith, M. J. *Mater. Res. Soc. Symp. Proc.* **1992**, *260*, 113−118.
(9) Jain, A.; Farkas, J.; Chi, K. M.; Hampden-Smith, M. J.; Kodas, T. T. *Adv. Met. ULSI Appl. 1992, Proc. Conf.* **1993**, *1992*, 82−89.
(10) Jain, A.; Kodas, T. T.; Jairath, R.; Hampden-Smith, M. J. *Proc. SPIE-Int. Soc. Opt. Eng.* **1993**, *2090*, 63−69.
(11) Jain, A.; Kodas, T. T.; Jairath, R.; Hampden-Smith, M. J. *J. Vac. Sci. Technol. B* **1993**, *11* (6), 2107−2113.
(12) Donnelly, V. M.; Gross, M. E. *J. Vac. Sci. Technol. A* **1992**, *11* (1), 66−77.
(13) Kim, S.; Park, J.-M.; Choi, D.-J. *Thin Solid Films* **1998**, *320* (1), 95−102.
(14) Kim, S.; Park, J.-M.; Choi, D.-J. *Thin Solid Films* **1998**, *315*, 229−237.
(15) Farkas, J.; Hampden-Smith, M. J.; Kodas, T. T. *J. Electrochem. Soc.* **1994**, *141* (12), 3539−3546.
(16) Farkas, J.; Hampden-Smith, M. J.; Kodas, T. T. *J. Electrochem. Soc.* **1994**, *141* (12), 3547−3555.
(17) Luisier, A.; Utke, I.; Bret, T.; Cicoira, F.; Hauert, R.; Rhee, S.-W.; Doppelt, P.; Hoffmann, P. *J. Electrochem. Soc.* **2004**, *151* (9), C590−C593.
(18) Cohen, S. L.; Liehr, M.; Kasi, S. *Appl. Phys. Lett.* **1992**, *60* (13), 1585−1587.
(19) Parmeter, J. E.; Petersen, G. A.; Smith, P. M.; Apblett, C. A.; Reid, J. S.; Norman, J. A. T.; Hochberg, A. K.; Roberts, D. A.; Omstead, T. R. *J. Vac. Sci. Technol. B* **1995**, *13* (1), 130−136.
(20) Norman, J. A. T.; Muratore, B. A.; Dyer, P. N.; Roberts, D. A.; Hochberg, A. K. *J. Phys. IV: Proc.* **1991**, *1*, C2/271-C2/278.
(21) Parmeter, J. E. *J. Phys. Chem.* **1993**, *97*, 11530−11541.
(22) Farkas, J.; Hampden-Smith, M. J.; Kodas, T. T. *J. Phys. Chem.* **1994**, *98*, 6753−6762.
(23) Data from NIST Standard Reference Database 69, June 2005 Release: NIST Chemistry WebBook. http://webbook.nist.gov/chemistry/ (June 2005).
(24) Becke, A. D. *J. Chem. Phys.* **1993**, *98*, 1372−1377.
(25) Lee, C.; Yang, W.; Parr, R. G. *Phys. Rev. B* **1988**, *37*, 785.
(26) Frisch, M. J. T.; et al. *Gaussian 03, Revision C.02*, Gaussian Inc: Wallinford, CT, 2004.
(27) Nachtigall, P.; Jordon, K. D.; Janda, K. C. *J. Chem. Phys.* **1991**, *95* (11), 8652−8654.
(28) Konecny, R.; Doren, D. J. *J. Chem. Phys.* **1997**, *106* (6), 2426−2435.
(29) Widjaja, Y.; Mysinger, M. M.; Musgrave, C. B. *J. Phys. Chem. B* **2000**, *104*, 2527−2533.
(30) Mui, C.; Wang, G. T.; Bent, S. F.; Musgrave, C. B. *J. Chem. Phys.* **2001**, *114* (22), 10170−10180.
(31) Barriocanal, J. A.; and Doren, D. J. *J. Phys. Chem. B* **2000**, *104*, 12269−12274.
(32) Barriocanal, J. A.; Doren, D. J. *J. Am. Chem. Soc.* **2001**, *123*, 7340−7346.
(33) Barriocanal, J. A.; Doren, D. J. *J. Vac. Sci. Technol. A* **2000**, *18* (4), 1959−1964.
(34) Konecny, R.; Doren, D. J. *Surf. Sci.* **1998**, *417*, 169−188.
(35) Konecny, R.; Doren, D. J. *J. Am. Chem. Soc.* **1997**, *119*, 11098−11099.
(36) Widjaja, Y.; Musgrave, C. B. *Phys. Rev. B* **2001**, *64* (20), 205303/1−205303/9.
(37) Widjaja, Y.; Musgrave, C. B. *Surf. Sci.* **2000**, *469*, 9−20.
(38) Wang, J.-H.; Lin, M. C. *Surf. Sci.* **2005**, *579*, 197−214.
(39) McLean, A. D.; Chandler, G. S. *J. Chem. Phys.* **1980**, *72*, 5639.
(40) Krishnan, R.; Binkley, J. S.; Seeger, R.; Pople, J. A. *J. Chem. Phys.* **1980**, *72*, 650.
(41) Blandeau, J. P.; McGrath, M. P.; Cusrtiss, L. A.; Radom, L. *J. Chem. Phys.* **1997**, *107*, 5016.
(42) Wachters, A. J. H. *J. Chem. Phys.* **1970**, *52*, 1033.
(43) Hay, P. J. *J. Chem. Phys.* **1977**, *91*, 1206.
(44) Raghavachari, K.; Trucks, G. W. *J. Chem. Phys.* **1989**, *91*, 1206.
(45) Binning, R. C., Jr.; Curtiss, L. A. *J. Comput. Chem.* **1995**, *11*, 1206.
(46) Curtiss, L. A.; McGrath, M. P.; Blandeau, J. P.; Davis, N. E.; Binning, R. C., Jr.; Radom, L. *J. Chem. Phys.* **1995**, *103*, 9104.
(47) McGrath, M. P.; Radom, L. *J. Chem. Phys.* **1991**, *94*, 511.
(48) Redhead, P. A. *Vacuum* **1962**, *12*, 203−211.
(49) Buemi, G. *J. Mol. Struct.* **2000**, *499*, 21−34.
(50) Tayyari, S. S.; Nejad, F. M.; Rahemi, H. *Spectrochim. Acta Part A* **2002**, *58*, 1669−1679.
(51) Andreassen, A. L.; Zebelman, D.; Bauer, S. H. *J. Am. Chem. Soc.* **1971**, *93*, 8−1152.
(52) Bertolassi, V.; Gilli, P.; Ferretti, V.; Gilli, G. *J. Am. Chem. Soc.* **1991**, *113*, 4917−4925.
(53) Minoura, Y.; Nagashima, N.; Kudoh, S.; Nakata, M. *J. Phys. Chem. A* **2004**, *108*, 2353−2362.
(54) Perrin, C. L.; Kim, Y.-J. *J. Am. Chem. Soc.* **1998**, *120*, 12641−12645.
(55) Bulanin, K. M.; Shah, A. G.; Fitzgerald, D. R.; Doren, D. J.; Teplyakov, A. V. *J. Phys. Chem. B* **2002**, *106*, 7286−7289.
(56) Willis, B., in preparation.